Proceedings of SMASIS08
ASME Conference on Smart Materials, Adaptive Structures and Intelligent Systems
October 28-30, 2008, Ellicott City, Maryland, USA

SMASIS2008-518

HYDRAULICALLY AMPLIFIED MAGNETOSTRICTIVE ACTUATOR FOR ACTIVE ENGINE MOUNTS

Suryarghya Chakrabarti
Smart Vehicle Concepts Center
Department of Mechanical Engineering
Ohio State University
Columbus, Ohio 43210
Email: chakrabarti.3@osu.edu

Marcelo J. Dapino*
Smart Vehicle Concepts Center
Department of Mechanical Engineering
Ohio State University
Columbus, Ohio 43210
Email: dapino.1@osu.edu

ABSTRACT

A bidirectional magnetostrictive actuator with millimeter stroke and a blocked force of $\pm$ 22 N has been developed based on a simple hydraulic magnification mechanism. The purpose of the actuator is to replace the electromagnetic actuator in active engine mounts. The Terfenol-D actuator has a flat free displacement response up to 200 Hz and a flat blocked force response over a frequency range of at least 10 to 500 Hz. The actuator promises to deliver a much broader frequency bandwidth than commercial electromagnetic actuators.

NOMENCLATURE

A_d cross sectional area of decoupler
A_e equivalent cross sectional area of upper chamber
A_L cross sectional area of driven (small) piston
A_P cross sectional area of drive (large) piston
A_t cross sectional area of the inertia track
β fluid's bulk modulus
β_{eff} effective volumetric modulus of fluid and fluid chamber
c_L viscous damping coefficient of small piston (due to O-rings)
c_P viscous damping coefficient of large piston (due to O-rings)
c damping coefficient of the inertia track
C_o effective volumetric stiffness coefficient of the various fluid chamber components
F_a blocked force produced by the Terfenol-D rod
I current in the drive coil
k_a internal stiffness of Terfenol D
k_{disk} stiffness of the disk spring
k_{pre} stiffness of the preload wave spring
K_r main stiffness of mount rubber
K_b bulge stiffness of mount rubber
m mass of the fluid in the inertia track
m_e engine mass
M_L effective mass of driven piston
M_p effective mass of drive piston
N number of turns in the coil
V_{ref} volume of hydraulic fluid
X_d actuator pushrod displacement
X engine displacement

INTRODUCTION

A typical engine mount has two main purposes. First, to isolate the high frequency engine vibrations from the chassis and second to prevent engine bounce from low frequency, high amplitude road excitations. The two functions are contradictory since the first requires the mount to be compliant and the second requires the mount to be stiff. This suggests that the mount must have frequency and amplitude dependent characteristics. To meet these requirements, various passive and semi-active mounts have been developed with significant vibration reduction (see, e.g., Yu et al. [1]). Despite these advances, the trend of increased

*Address all correspondence to this author.

engine power combined with lighter vehicle frames poses vibration isolation problems which passive mounts cannot adequately address. Hence, significant emphasis is now placed on investigating designs and methods to develop effective active mounts. Lee et al. [2] developed an electromagnetic actuator with a bandwidth of 75 Hz. Gennesseaux [3] discusses a variable reluctance linear electric motor with in-built close loop control to address actuator nonlinearities. Although active mounts with electromagnetic actuators can achieve significant vibration reduction , their performance is restricted to low frequencies, typically below 80 Hz. Actuators capable of broader frequency bandwidth are thus necessary.

Most of the smart material induced strain actuators capable of broadband response have a very limited stroke with peak strains on the order of 1200 ppm. Given the size restrictions of the automotive mount, a displacement amplification mechanism is necessary when employing smart materials. Niezrecki et. al. [4] have summarized some of the displacement amplification techniques found in the literature. Most of these mechanisms like stacking or using mechanical levers are too bulky to be used in an active mount. Another way to amplify the motion of smart material actuators is by using a hydraulic fluid. Hydraulic amplification can also be achieved either by direct amplification based on pistons of different areas or by using smart material pumps driven at high frequency along with fluid rectification valves. Various pumps have been developed using both magnetostrictive [5] and piezoelectric materials [6]. The current designs are too bulky and complex for use in engine mounts due to the presence of various pumping components, an accumulator, check valves, direction control valve and a piston type hydraulic actuator. Hence, direct hydraulic amplification mechanisms are more attractive for designing smart material actuators for automotive engine mounts.

Ushijima and Kumakawa [7] developed a piezo-hydraulic actuator with a stroke of 70 μm which uses the hydraulic fluid in the mount itself for amplification. Shibayama et al. [8] developed a hydraulically amplified piezo actuator having a stroke of 0.3 mm with considerable reduction in vibration transmission. The hydraulic fluid used for amplification was separately sealed from the fluid in the mount. However, the required voltages are very large. The present work aims at creating a compact bidirectional magnetostrictive actuator coupled with a hydraulic gain to be used as an actuator in active engine mounts.

ACTUATOR DESIGN

Estimation of Actuator Requirements

The first step is to quantify the actuator requirements of a generic active mount. This is done by using a model similar to that developed by Lee et al. [2] (Figure 1). In this model, the transfer function of the actuator displacement to the engine displacement is given by

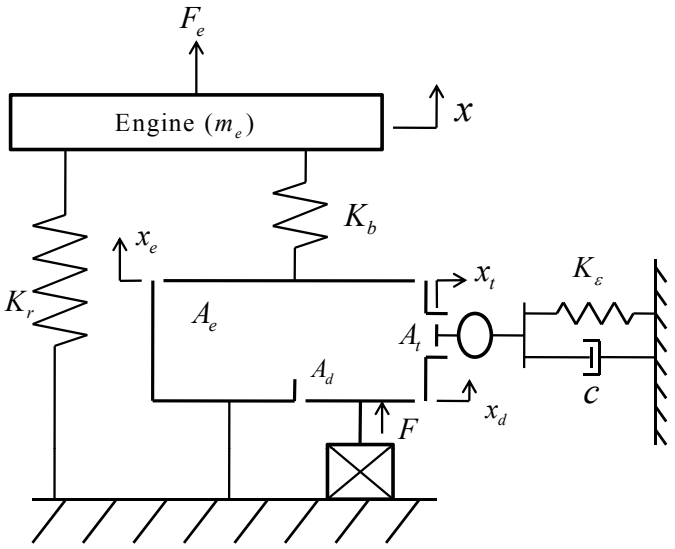

Figure 1. SCHEMATIC OF THE ACTIVE MOUNT MODEL (LEE ET. AL. [2]).

Table 1. PARAMETERS OF THE ACTIVE MOUNT

Parameter	Value
Main rubber stiffness (K_r)	127.4×10^3 N/m
Bulge stiffness of the rubber (K_b)	313.6×10^3 N/m
Compliance of the lower chamber (K_ε)	2.0 N/m
Equivalent cross-sectional area of the upper chamber (A_e)	4123 mm^2
Decoupler area	1662 mm^2
Cross-sectional area of the inertia track	50 mm^2
Fluid mass in the inertia track (m)	12.5 g
Damping coefficient in the inertia track	0.08 Ns/m

$$\frac{X_d}{X}(s) = \left[\left(1+\frac{K_r}{K_b}\right)\frac{A_e}{A_d} + \frac{K_r A_t^2}{A_e A_d\,(ms^2+cs+K_\varepsilon)}\right]. \quad (1)$$

Table 1 summarizes the values of the parameters used in our simulations, which coincide with the parameters used by Lee et al. [2].

Figure 2 shows the magnitude of the frequency response. The response remains almost constant in the frequency range

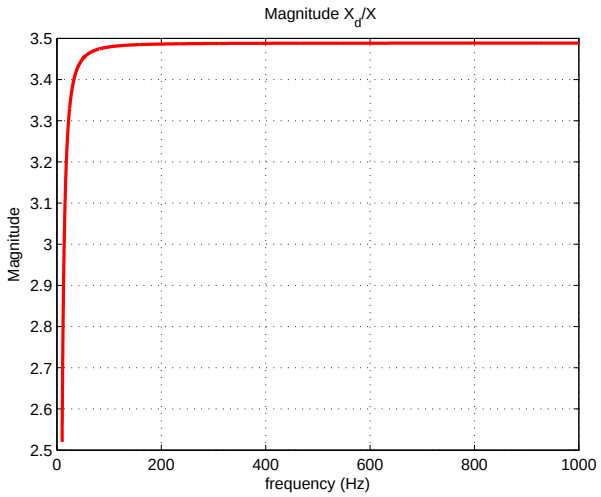

Figure 2. FREQUENCY RESPONSE (X_d/X) (MAGNITUDE ONLY).

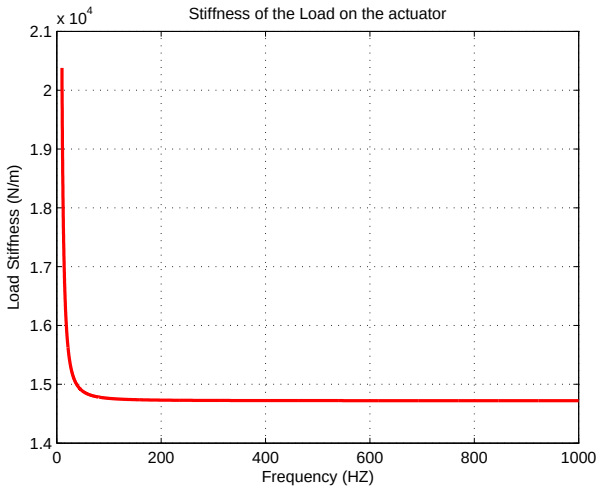

Figure 3. LOAD STIFFNESS F/X_d (MAGNITUDE ONLY).

from 100 to 1000 Hz. To estimate the actuator displacement requirement from this plot, it is first necessary to estimate the engine displacement excitation which is the input to the model. Holt and Rao [9] assumed an excitation of amplitude 0.3 mm over the range 0 to 100 Hz and 0.01 mm over the range 100 to 200 Hz. Ohadi and Maghsoodi [10] assumed an excitation of amplitude 1.0 mm in the frequency range 0 to 6 Hz and 0.05 mm at higher frequencies. Lee et al. [2] measured the engine vibration amplitude in the idling state to be 0.22 mm. Kyprianou et. al. [11] assumed excitations with r.m.s amplitudes ranging from 0.005 mm at higher frequencies to 0.33 mm at lower frequencies. In this paper the engine vibration amplitude is assumed to be 0.5 mm at the idling frequency (20 Hz), decaying linearly to 0.1 mm at 100 Hz and then decreasing linearly to 0.05mm at 1000 Hz. From this, the displacement requirement of the actuator is calculated from the transfer function (1) to be 1.6 mm at 20 Hz, 0.35 mm at 100 Hz, and 0.175 mm at 1000 Hz.

The transfer function between the actuator force and engine displacement can be written as

$$\frac{F}{X}(s) = \left(\frac{A_d}{A_e}\right) K_r, \tag{2}$$

from where the force requirement can be estimated as 26 N at idling conditions. It is emphasized that these requirements are for complete cancellation of the engine vibrations. Actuators with capabilities lower than these could also provide significant (although not complete) vibration reduction. The force generation capability of the proposed actuator will be decided by the dimensional constraints on the Terfenol-D rod. In this case a Terfenol-D rod of 0.5 in diameter and 2 in length has been chosen. This means that the expected blocked force of the rod is 4560 N (assuming E = 30 GPa) and its free stroke is 60 μm (assuming λ = 1200 ppm).

Actuator Gain

One of the key factors in the performance of any displacement amplified actuator is the kinematic gain. The calculation of kinematic gain for any induced strain actuator cannot be done simply by dividing the required displacement by the actuator free displacement. The maximum strain is obtained when the load is zero and the maximum load is supported when the displacement is zero. Thus, calculation of the kinematic gain must incorporate loading effects. Giurgiutiu et al. [12] derived that to get maximum energy output from a displacement amplified induced strain actuator, one must operate it at its optimal gain,

$$G_{opt} = 1/\sqrt{r}, \tag{3}$$

where r is the ratio of load stiffness to the smart material stiffness. The effective stiffness of the load and actuator is obtained by dividing (2) by (1). Figure 3 shows the load stiffness as a function of frequency. Since the actuator requirements are most stringent at the idling frequency, the stiffness match principle is enforced at that frequency and the value of the gain is found to be $G_{opt} = 69$.

Thus the actuator is designed such that there is a fluid chamber with the large driving piston at one end and a small diameter load piston at the other. Figure 4 shows the physical actuator and

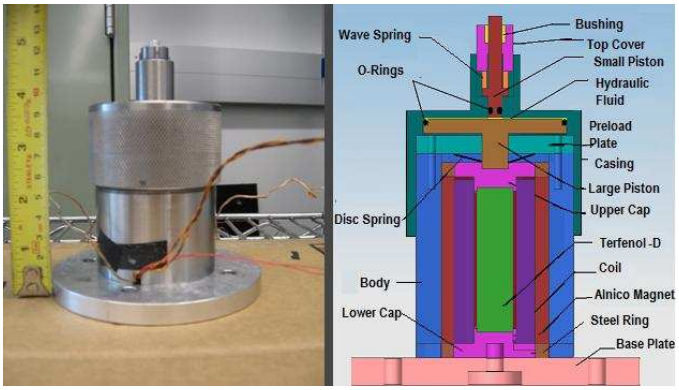

Figure 4. PHYSICAL ACTUATOR (LEFT) AND CUTOUT (RIGHT).

a cutout showing the actuator components. The exact ratio of piston areas in this design is 69.6.

Magnetic Circuit and Preload

The magnetic circuit consists of three cylindrical Alnico permanent magnets of ID 1.125" and OD 1.5", a AWG 20 wire coil for generating the dynamic field, iron pieces for flux return and a Terfenol D rod. The coil has an ID of 0.6" and an OD of 1". The permanent magnet provides the required magnetic bias to achieve bidirectional motion.

The mechanical preload on the Terfenol-D rod is obtained from two sources. First, through the wave spring on top whose force is then magnified by the fluid before being exerted on the Terfenol-D rod, and second through a disc spring located just above the magnetic circuit. The advantage of having a major part of the preload through the fluid is that the fluid remains in compression all the time thus reducing chances of cavitation. The fluid is sealed on both the ends by two dynamic o-rings (#6 for the smaller piston and #32 for the larger piston). Table 2 gives the specifications for the different components of the magneto-hydraulic actuator (MHA).

EXPERIMENTAL RESULTS

Two kinds of tests were conducted on the actuator, free displacement tests (no external load) and blocked force tests (no displacement of the output pushrod). Both responses in the frequency domain were obtained at constant current with the help of a controller and a feedback loop. Figure 5 shows a schematic of the experimental setup used to conduct the tests. The signal from the signal generator is amplified and fed to the MHA. The feedback from the amplifier's current monitor enables the controller to adjust the output of the signal generator to achieve the required level of constant current to drive the MHA.

Table 2. DIFFERENT COMPONENTS USED IN THE ACTUATOR

Component	Specification
Length of Terfenol-D rod	2 in
Diameter of Terfenol-D rod	0.5 in
Alnico magnet (ID $\times$ OD $\times$ L)	(1.125 in $\times$ 1.5 in $\times$ 2.25 in)
Mass of larger Piston	74.67 g
Mass of smaller Piston	2.30 g
Volume of fluid(DTE 25)	1.30 c.c
Wave spring stiffness	2.27×10^3 N/m
Finger disc spring Stiffness	2.25×10^5 N/m

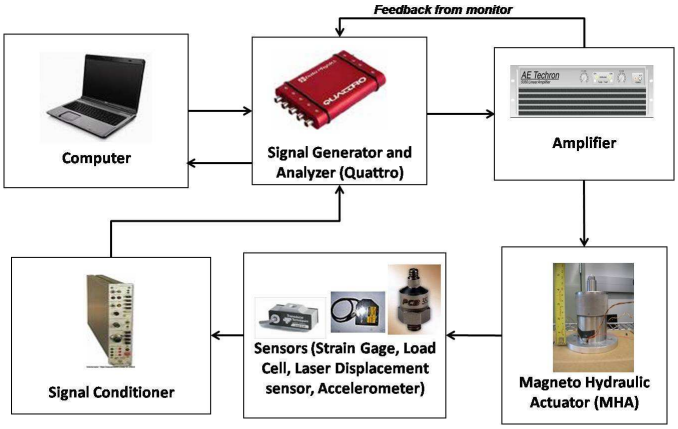

Figure 5. SCHEMATIC OF THE EXPERIMENTAL SETUP.

Free Displacement

The free displacement was measured with a laser displacement sensor. Figure 6 shows the magnitude and phase (with respect to current) of the free displacement.

The displacement frequency response is fairly flat up to 200 Hz. The actuator generates a free displacement level of ± 1 mm up to 200 Hz. The phase decreases linearly up to 350 Hz. Figure 7 shows that the -3 dB bandwidth of the actuator is 280 Hz.

Blocked Force

The blocked force test was done by blocking the actuator's output pushrod. A flat blocked force response was obtained over the entire test frequency range (10 to 500 Hz). Figure 8 shows the measured blocked force response. A blocked force of ± 22 N

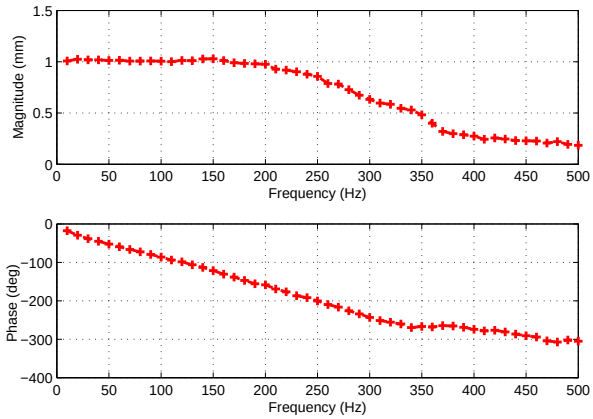

Figure 6. MEASURED FREE DISPLACEMENT MAGNITUDE AND PHASE(WITH RESPECT TO CURRENT).

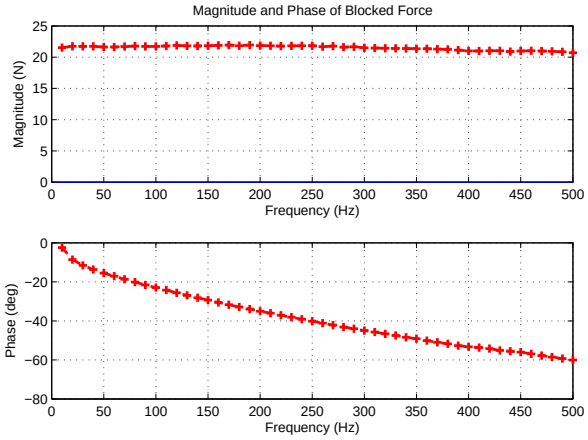

Figure 8. MEASURED BLOCKED FORCE RESPONSE.

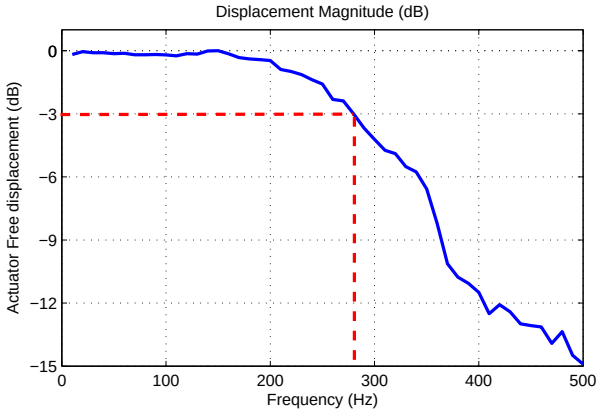

Figure 7. 3 DB BANDWIDTH OF THE ACTUATOR.

is delivered over the entire frequency range.

THEORY

A two-degree of freedom dynamic model was developed as shown in Figure 9. Assuming no compliance of the fluid chamber, at any given instant of time the volumetric displacement of the hydraulic fluid can be given as

$$\Delta V = A_p x_p - A_L x_L. \tag{4}$$

However, it is expected that the volumetric stiffness of the different elements in the fluid chamber would play a critical role in the performance of the actuator. Hence a volumetric stiffness coefficient (C_o) is introduced, to be estimated experimentally. Now

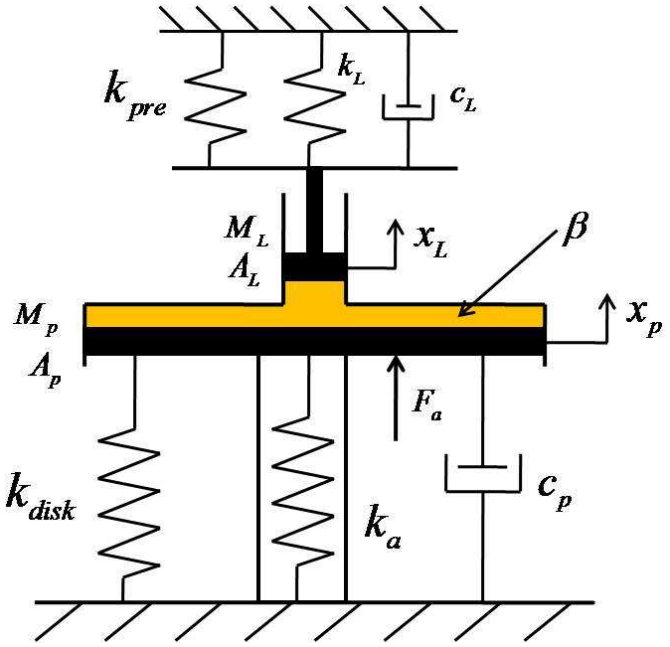

Figure 9. SCHEMATIC OF THE ACTUATOR MODEL.

the volumetric change can be written as

$$\Delta V = A_p x_p - A_L x_L - \frac{\Delta p}{C_o}. \tag{5}$$

The pressure in the fluid can be linearized for small volumetric changes and can be written as

$$\Delta p = \beta \frac{\Delta V}{V_{ref}}. \tag{6}$$

Substitution of ΔV from (5) into (6) and solution for Δp gives

$$\Delta p = \underbrace{\left(\frac{C_o \beta}{C_o V_{ref} + \beta} \right)}_{\beta_{eff}} (A_p x_p - A_L x_L). \tag{7}$$

If the volumetric stiffness of the chamber is very large then the coefficient β_{eff} is approximately equal to β / V_{ref}. It is noted that β_{eff} is the effective volumetric modulus of the fluid and fluid chamber assembly and does not have the same units as β.

The dynamic equations for the larger and smaller piston can now be written as

$$M_p \ddot{x_p} + c_p \dot{x_p} + \underbrace{(k_a + k_{disk})}_{k_{p_{eff}}} x_p = -\beta_{eff} (A_p x_p - A_L x_L) A_p + F_a, \tag{8}$$

$$M_L \ddot{x_L} + c_L \dot{x_L} + \underbrace{(k_{pre} + k_L)}_{k_{L_{eff}}} x_L = \beta_{eff} (A_p x_p - A_L x_L.) A_L. \tag{9}$$

The force generated by the Terfenol-D rod can be expressed in terms of the drive current as

$$F_a = \underbrace{(qK_aN)}_{\theta} I. \tag{10}$$

where q is the piezomagnetic coefficient and N is the number of turns in the driving coil.

From equations (8)-(10), the transfer functions X_p/I and X_L/I can be found in the Laplace domain as

$$\frac{X_p}{I}(s) = \left(\frac{M_L s^2 + c_L s + k_{L_{eff}}}{\left(M_p s^2 + c_p s + k_{p_{eff}}\right)\left(M_L s^2 + c_L s + k_{L_{eff}}\right) - \beta_{eff}^2 A_L^2 A_p^2} \right) \theta, \tag{11}$$

$$\frac{X_L}{I}(s) = \left(\frac{\beta_{eff} A_L A_p}{\left(M_p s^2 + c_p s + k_{p_{eff}}\right)\left(M_L s^2 + c_L s + k_{L_{eff}}\right) - \beta_{eff}^2 A_L^2 A_p^2} \right) \theta. \tag{12}$$

The coefficient β_{eff} was estimated experimentally to be 7.78×10^{12} N/m^5. Figures 10 and 11 show the simulated displacements for the small and large piston.

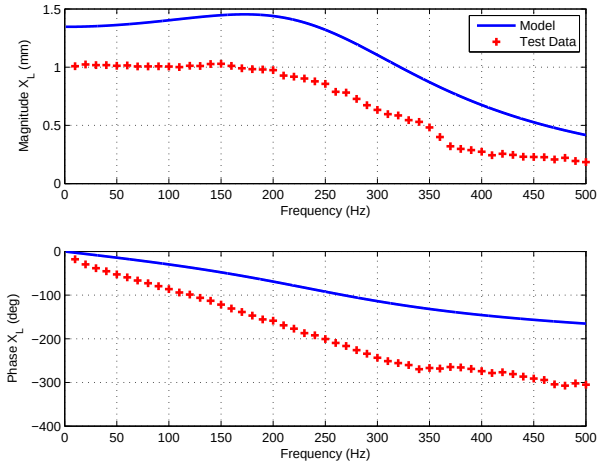

Figure 10. SMALL PISTON DISPLACEMENT, MAGNITUDE AND PHASE WITH RESPECT TO CURRENT.

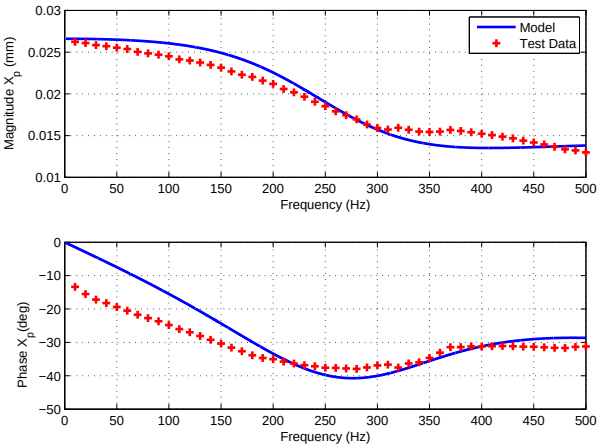

Figure 11. LARGE PISTON DISPLACEMENT, MAGNITUDE AND PHASE WITH RESPECT TO CURRENT.

Electrical Impedance

The voltage U across the coil can be expressed as

$$U = (R + sL_s) I + \theta s x_p, \tag{13}$$

therefore U/I can be written as

$$\frac{U}{I} = (R + sL_s) + \theta s \frac{x_p}{I}, \tag{14}$$

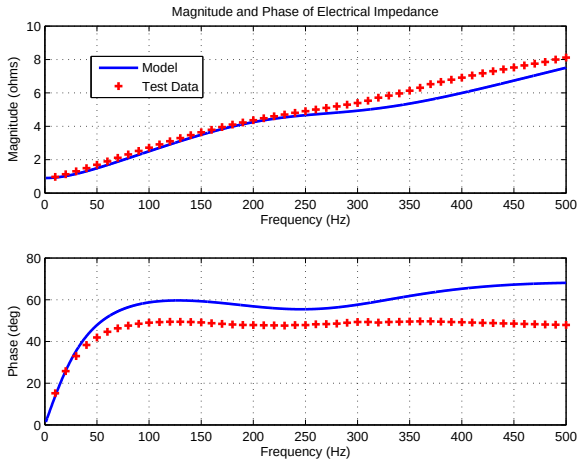

Figure 12. BODE PLOT OF EXPERIMENTAL AND CALCULATED ELECTRICAL IMPEDANCE.

where X_p/I is given by (11). Figure 12 shows the measured and calculated electrical impedance function.

It can be seen in Fig. 10 that the linear model grossly over predicts the performance of the actuator. The reduction in the actual performance of the actuator occurs mainly due to friction at the seals (primarily the small piston's o-ring). Thus the linear model described above was modified by including frictional forces at both the upper and the lower pistons. The modified system equations have the form

$$\begin{aligned} &M_p\ddot{x_p} + c_p\dot{x_p} + k_{p_{eff}}x_p + fr_p(sgn(\dot{x_p})) \\ &= \beta_{eff}\,(A_L x_L - A_p x_p)A_p + F_a, \end{aligned} \tag{15}$$

$$M_L\ddot{x_L} + c_L\dot{x_L} + k_{L_{eff}}x_L + fr_L(sgn(\dot{x_L})) = \beta_{eff}\,(A_p x_p - A_L x_L)A_L. \tag{16}$$

The values of fr_p and fr_L were found experimentally to be 96.78 N and 2.08 N, respectively. The result for X_L, X_p and electrical impedance obtained by numerically solving equations (15) and (16) are shown in Figures 13-15.

The nonlinear model which considers frictional forces provides a much better description of the measurements compared to the linear model. There are discrepancies in the phase which could be due to the assumed linear force-current relationship for the Terfenol-D rod.

CONCLUSION

This paper presents the design and modeling of a hydraulically amplified magnetostrictive actuator developed for use in an

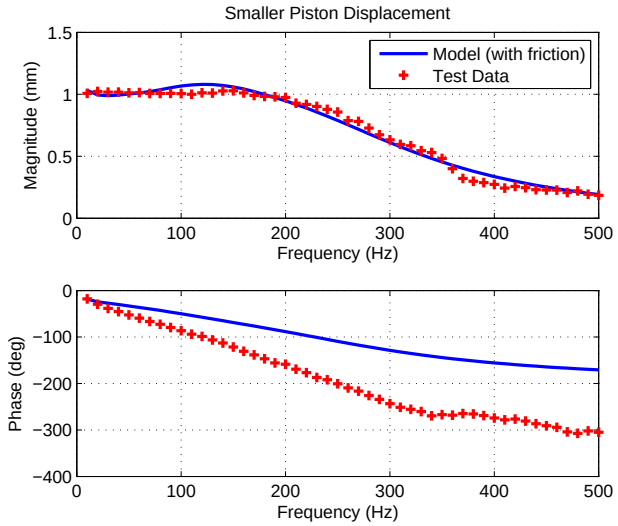

Figure 13. BODE PLOT OF SMALL PISTON DISPLACEMENT WITH RESPECT TO CURRENT.

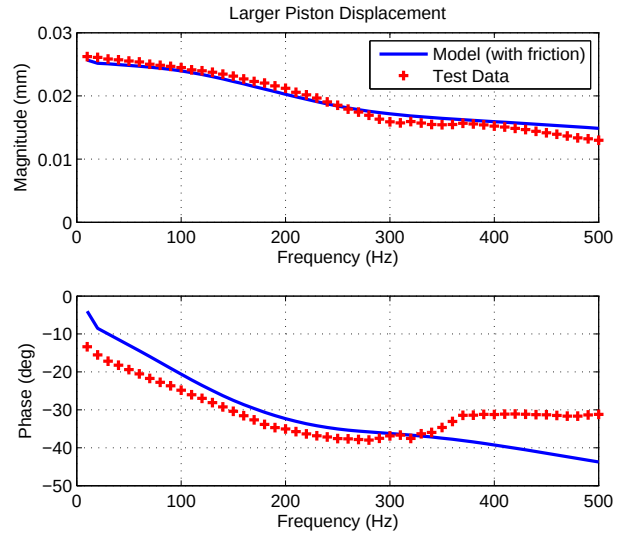

Figure 14. BODE PLOT OF LARGE PISTON DISPLACEMENT WITH RESPECT TO CURRENT.

active engine mount. The paper discusses the techniques used for estimating the actuator force and displacement requirement. The actuator was tested at constant current and its free displacement and blocked force characteristics were measured. The results show that the proposed magneto-hydraulic actuator is suitable for use in active engine mounts. A linear system model and subsequently a nonlinear model considering frictional forces

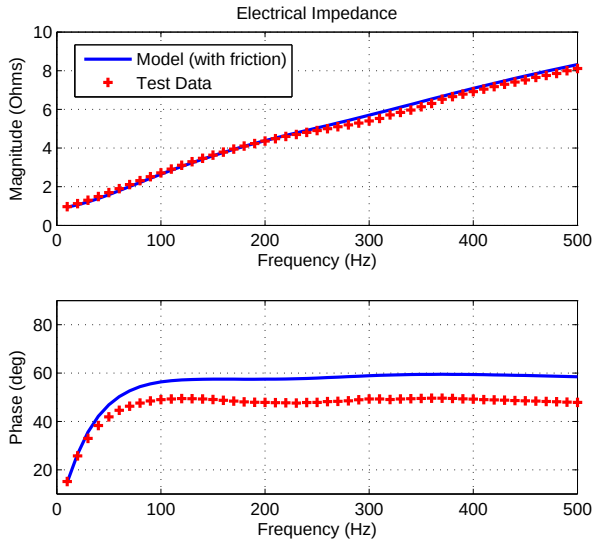

Figure 15. BODE PLOT OF EXPERIMENTAL AND CALCULATED ELECTRICAL IMPEDANCE, MODIFIED MODEL.

were developed. The model calculations for the two piston displacements and electrical impedance were compared with the experimental results. The linear model over-predicts the measured actuator performance since it does not include frictional effects. The nonlinear model on the other hand predicts the actuator behavior much better both in terms of phase and magnitude.

ACKNOWLEDGMENT

We are grateful to the member organizations of the Smart Vehicle Concepts Center (www.SmartVehicleCenter.org) and the National Science Foundation Industry/University Cooperative Research Centers program (www.nsf.gov/eng/iip/iucrc) for supporting this work.

REFERENCES

[1] Yu, Y., Naganathan, N., and Dukkipati, R., 1999. "A literature review of automobile engine mounting systems". In Mechanisms and Machines Theory, Vol. 36, pp. 123–142. PDF file.

[2] Lee, Y., and Lee, C., 2002. "Dynamic analysis and control of an active engine mount system". In Proc Instn Mech Engrs Part D: J Automobile Engineering, Vol. 216, pp. 921–931.

[3] Gennesseaux, A., 1995. "A new generation of engine mounts". *SAE*(951296).

[4] Niezrecki, C., Brei, D., Balakrishnan, S., and Moskalik, A., 2001. "Piezoelectric actuation: State of the art". *Shock and Vibration Digest*, **33**, July, pp. 269–280.

[5] Ellison, J., Sirohi, J., and Chopra, I., 2004. "Design and testing of a bidirectional magnetostrictive-hydraulic hybrid actuator". In Proc. SPIE, Vol. 5390, pp. 483–494.

[6] Mauck, L. D., and Lynch, C. S., 2000. "Piezoelectric hydraulic pump development". *Journal of Intelligent Material Systems and Structures*, **11**, October, pp. 758–764.

[7] Ushijima, T., and Kumakawa, S., 1993. "Active engine mount with piezo-actuator for vibration control". *SAE*(930201).

[8] Shibayama, T., Ito, K., Gami, T., Oku, T., Nakajima, Z., and Ichikawa, A., 1995. "Active engine mount for a large amplitude of engine vibration". *SAE*(951298).

[9] Holt, J., Rao, M., Blough, J., and Gruenberg, S., 2007. "Time history-based excitation in the dynamic characterization of automotive elastomers". In Proc. IMechE Part D: J. Automobile Engineering, Vol. 221, pp. 271–284.

[10] Ohadi, A., and Maghsoodi, G., 2007. "Simulation of engine vibration on nonlinear hydraulic engine mounts". *Journal of Vibration and Accoustics*, **129**, August, pp. 417–424.

[11] Kyprianou, A., Giacomin, J., Worden, K., Heidrich, M., and Bocking, J., 2000. "Differential evolution based identification of automotive hydraulic engine mount model parameters". In Proc. Instn. Mech. Engrs., Vol. 214.

[12] Giurgiutiu, V., Chaudhry, Z., and Rogers, C., 1995. "Stiffness issues in the design of isa displacement amplification devices". In Proc. SPIE, Vol. 2443, pp. 105–119.